Supporting Information

Controlling pH-regulated Bionanoparticles Translocation through Nanopores with Polyelectrolyte Brushes

Li-Hsien Yeh,[1+] Mingkan Zhang,[2+] Sang W. Joo,[3] Shizhi Qian,[2,3*] and Jyh-Ping Hsu,[4,*]

[1]Department of Chemical and Materials Engineering, National Yunlin University of Science and Technology, Yunlin 64002, Taiwan

[2]Institute of Micro/Nanotechnology, Old Dominion University, Norfolk, VA 23529, USA

[3]School of Mechanical Engineering, Yeungnam University, Gyongsan 712-719, South Korea

[4]Department of Chemical Engineering, National Taiwan University, Taipei 10617, Taiwan

* Corresponding authors:
E-mails: sqian@odu.edu (Shizhi Qian), jphsu@ntu.edu.tw (Jyh-Ping Hsu)

---

1. Boundary Conditions, Forces Acting on the Soft NP, Numerical Implementation, and Code Validation

The boundary conditions associated with eqs 3-6 of the text are based on the following assumptions. (i) The ionic concentrations on both ends of the two reservoirs reach their bulk values (i.e., $c_j = C_{j0}$), and the corresponding electric potentials are $V(cis)=0$ and $V(trans)=V_0$. A normal flow without external pressure gradient is specified on both ends of the two reservoirs. (ii) The rigid core surface of the soft NP is non-slip ($\mathbf{u} = u_p \mathbf{e_z}$), ion-impenetrable ($\mathbf{n} \cdot \mathbf{N}_j = \mathbf{n} \cdot (\mathbf{u} c_j)$),[1] and uncharged ($-\varepsilon_f \mathbf{n} \cdot \nabla V = 0$), where $\mathbf{n}$ is the unit outer normal vector. (iii) The rigid surface of the membrane is non-slip ($\mathbf{u}=\mathbf{0}$), ion-impenetrable ($\mathbf{n} \cdot \mathbf{N}_j = 0$), and uncharged ($-\varepsilon_f \mathbf{n} \cdot \nabla V = \sigma_w = 0$), where σ_w is its charge

density. (iv) The electric potential, electric field, ionic concentration, and flow field are all continuous on the two ion-penetrable layer/liquid interfaces.[2] (v) Slip boundary condition for the flow field, insulation boundary condition for the potential, and zero normal ionic fluxes are imposed on the side boundaries of the two reservoirs, which are far away from the nanopore.

The forces acting on the soft nanoparticle (NP) include the electrophoretic force $\mathbf{F_E}$ and the hydrodynamic drag $\mathbf{F_H}$. In our case, only the *z* components of these forces, F_E and F_H, need to be considered. These values can be obtained by integrating the Maxwell stress tensor, $\boldsymbol{\sigma}^{\mathbf{E}} = \varepsilon_f \mathbf{EE} - (1/2)\varepsilon_f (\mathbf{E}\cdot\mathbf{E})\mathbf{I}$, and the hydrodynamic stress tensor, $\boldsymbol{\sigma}^{\mathbf{H}} = -p\mathbf{I} + 2\mu\boldsymbol{\Delta}$, over the soft NP surface, Ω_p. Here, $\mathbf{I}$, $\boldsymbol{\Delta} = [\nabla\mathbf{u} + (\nabla\mathbf{u})^{\mathbf{T}}]/2$, and the superscript $\mathbf{T}$ are the unit tensor, the rate of deformation tensor, and matrix transpose, respectively. It can be shown that[1,3]

$$F_E = \int_{\Omega_p} \varepsilon_f \left[\frac{\partial V}{\partial r}\frac{\partial V}{\partial z} n_r - \frac{1}{2}\left(\left(\frac{\partial V}{\partial r}\right)^2 + \left(\frac{\partial V}{\partial z}\right)^2 \right) n_z \right] d\Omega_p , \qquad \text{(R1)}$$

$$F_H = \int_{\Omega_p} \left[\mu\left(\frac{\partial u}{\partial z} + \frac{\partial v}{\partial r} \right) n_r + n_z \left(-p + 2\mu\frac{\partial v}{\partial z} \right) \right] d\Omega_p . \qquad \text{(R2)}$$

Here, n_r and n_z are the *r*- and the *z*- components of the unit normal vector, **n**, respectively. Under the quasi-steady state assumption, the translocation velocity of the soft NP, u_p, can be determined by $F_E + F_H = 0$.[1,4]

The non-linear, highly coupled equations, eqs 2-6, and the associated boundary conditions

described in the text are numerically solved by COMSOL Multiphysics (version 3.5a, www.comsol.com), a commercial finite element method based software operated in a high-performance cluster. Finer mesh is generated around the charged soft NP and Polyelectrolyte (PE)-modified nanopore to capture their electric double layers (EDLs). All the results presented are ensured to be convergent and mesh-independent. Typically, using a total number of ca. 130,000 meshes is sufficient. More details about the implementation of the software can be found in our previous studies.[5]

The applicability of the numerical scheme adopted is first examined by considering the electrophoresis of an isolated, soft spherical particle in an infinite electrolyte solution, which was solved analytically by Ohshima[6] under the conditions of low surface potential and constant fixed charged density ρ_p. Assuming $\kappa(a-d) >> 1$, $\kappa d >> 1$, $(a-d)/\lambda_p >> 1$, $d/\lambda_p >> 1$, and $\overline{Q} << (\kappa(a-d))^2/2$,[6] it can be shown that the electrophoretic velocity of the soft particle, u_p, is

$$\frac{u_p^*}{E^*} = \frac{\overline{Q}\lambda_p{}^2}{(a-d)^2}\left[1+\frac{2}{3}\left(\frac{1}{\kappa\lambda_p}\right)^2\left(\frac{1+1/(2\kappa\lambda_p)}{1+1/(\kappa\lambda_p)}\right)\left(1+\frac{(a-d)^3}{2a^3}\right)\right]. \qquad \text{(R3)}$$

Here, $u_p^* = u_p(\mu a F^2/\varepsilon_f R^2 T^2)$, $E^* = E(aF/RT)$, and $\overline{Q} = \overline{\rho}_p a^2 F/(\varepsilon_f RT)$. $\overline{\rho}_p = \int_{V_p}\rho_p dV_p / \int_{V_p} dV_p$ is the volume-averaged charged density in the soft layer of the soft particle with V_p being the volume of that layer; $\kappa^{-1} = \lambda_D = (\varepsilon_f RT/F^2\sum_{j=1}^{N} z_j^2 C_{j0})^{1/2}$ is the Debye length. Figure S1 shows the variations of the normalized volume-averaged charged

density, $\overline{Q}$, and the corresponding normalized particle velocity, u_p^*, as a function of the scaled Debye length κa. Figure S1a shows that $|\overline{Q}|$ is not a constant, and increases with increasing κa (or salt concentration), which is expected. As can be seen in Figure S1b, our numerical results (solid line) are in good agreement, in general, with the analytical results (circles) based on eq R3,[6] indicating that the performance of the present numerical scheme is satisfactory. Note that our numerical results are slightly larger than the corresponding analytical results, which arises from that ρ_p is position-dependent in our case, but not a constant assumed in the derivation of eq R3.[6]

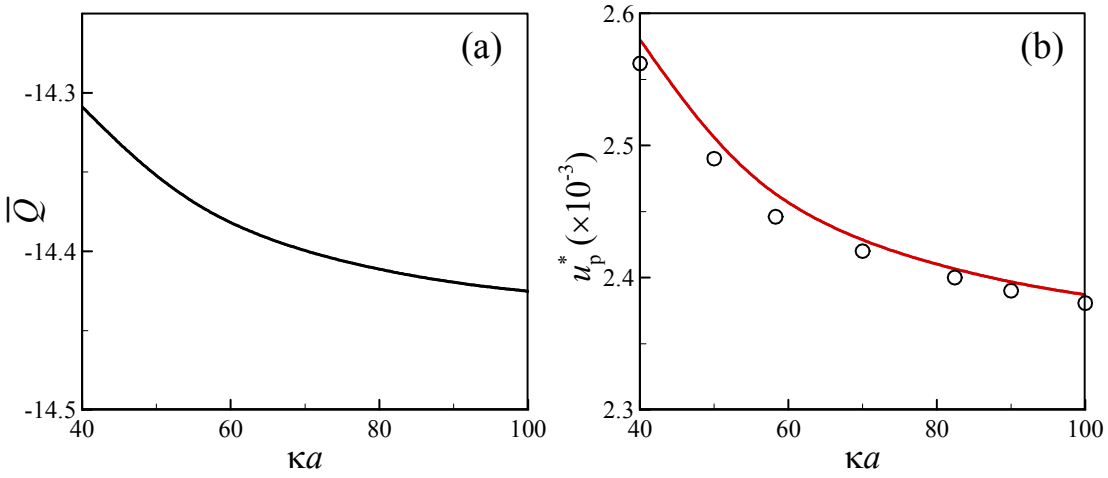

Figure S1. Normalized volume-averaged charge density of the soft layer in the soft particle, $\overline{Q}$, (a), and its normalized particle velocity, u_p^*, (b), as a function of κa for the case where $a/\lambda_p = 19.4$, d/a=0.5, and $\mathrm{pH}_0 = 6$. Lines: present numerical results; circles: approximation solution based on eq R3.

2. Influences of Background Solution Properties on the Local pH in Soft NP

The influence of the background salt concentration C_{KCl} and the background solution pH_0 on the distribution of local pH ($=-\log[\mathrm{H}^+]$) in the soft NP at various particle positions z_p are depicted in Figure S2. This figure shows that if the soft NP is far away from the PE-modified nanopore ($z_p = -60\,\mathrm{nm}$), the distribution of H^+ is not influenced by the nanopore. On the other hand, as it enters the PE-modified nanopore ($z_p = 0$ and -10 nm), that distribution becomes highly non-uniform. In this case, the local pH near the lower side of the soft NP is smaller than that near its upper side; that is, the concentration of H^+ is higher in the former region. As discussed in Figure 2 of the text, this can be attributed to the combined effects of the double-layer polarization (DLP),[7] due to the motion of the soft NP, and the ion concentration polarization (CP) occurring in the PE-modified nanopore.[8] The former results in the convective motion of counterions (H^+ and K^+) inside the electric double layer (EDL) of the soft NP migrating from its upper side to lower side.[9] The latter induces an enrichment (depletion) of ions occurring at the *cis* (*trans*) side of the nanopore. As will be shown later, the distribution of counterions (cations) inside a cations-selective nanopore is highly asymmetric. In addition, because the drop in the applied voltage concentrates mainly within the nanopore, the electric field inside is extremely high, so is the degree of DLP. These two effects makes the local pH in the soft NP highly asymmetric as its center completely enters the PE-modified nanopore ($z_p = 0$), as illustrated in Figure S2c, f, and i.

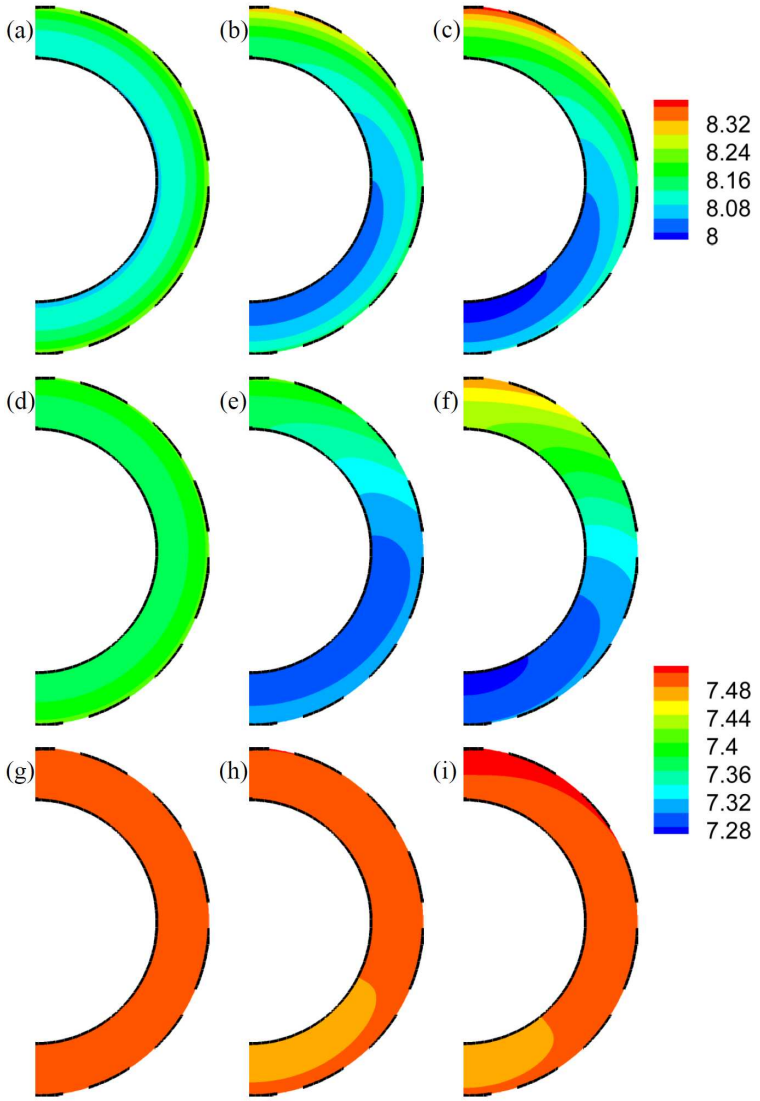

Figure S2. Spatial distribution of local pH value in the soft NP for the case of Figure 2 in the text at $z_p = -60$, (a), (d), and (g), -10, (b), (e), and (h), and 0 nm, (c), (f), and (i). (a)-(c): $C_{\mathrm{KCl}} = 50\ \mathrm{mM}$ and $\mathrm{pH}_0 = 8.5$; (d)-(f): $C_{\mathrm{KCl}} = 50\ \mathrm{mM}$ and $\mathrm{pH}_0 = 7.5$; (g)-(i): $C_{\mathrm{KCl}} = 1000\ \mathrm{mM}$ and $\mathrm{pH}_0 = 7.5$.

3. Enhanced Positive Flow Field at PE-modified Nanopore Mouth

Figure S3 shows the flow field, (a) and (d), and the spatial distribution of the net cation concentration ($c_1 + c_2$), (b) and (c), near a PE-modified nanopore. For comparison, the results for the corresponding charged solid-state nanopore are also presented. Figure S3b and c

reveals that ($c_1 + c_2$) is high in the vicinity of the nanopore surface in the case of a solid-state nanopore, but remains high in the whole polyelectrolyte (PE) layer of the PE-modified nanopore. Because the overlapping of EDL in the PE-modified nanopore is more significant than that in the corresponding solid-state nanopore, the ion CP becomes more significant in the former, resulting in a highly asymmetric distribution of net counterions (cations) in the PE-modified nanopore, as seen in Figure S3b. As a result, a significant enrichment (depletion) of counterions, occurs in the PE layer on the *cis* (*trans*) side of the PE-modified nanopore, which is capable of inducing a cations-rich field at the nanopore mouth to electrostatically attract the soft NP and, therefore, to enhance its capture velocity. As seen in Figure S3a, due to a significant ion CP occurring in the PE-modified nanopore, the fluid in the *trans* reservoir flows along the membrane surface; part of it funnels the nanopore towards the *cis* reservoir (EOF), and the rest flows back towards the its end. The fluid in the *cis* reservoir flows from its end towards the nanopore mouth and merges with the fluid flowing out from the nanopore. Note that the fluid inside both reservoirs flows in a direction opposite to that of the EOF inside the PE-modified nanopore. This is not observed in the case of a solid-state nanopore, as shown in Figure S3d. The EOF slows down the translocation velocity of the soft NP inside the nanopore. In addition, the positive fluid flow in the *cis* reservoir is capable of enhancing the capture rate of the soft NP by the nanopore. These suggest that the proposed PE-modified nanopore has the potential of being applied in nanopore-based sensing technology by raising

both the capture rate and capture velocity of a sensing entity and simultaneously reducing its translocation velocity in the nanopore, so that the sensing resolution can be enhanced at high throughput.

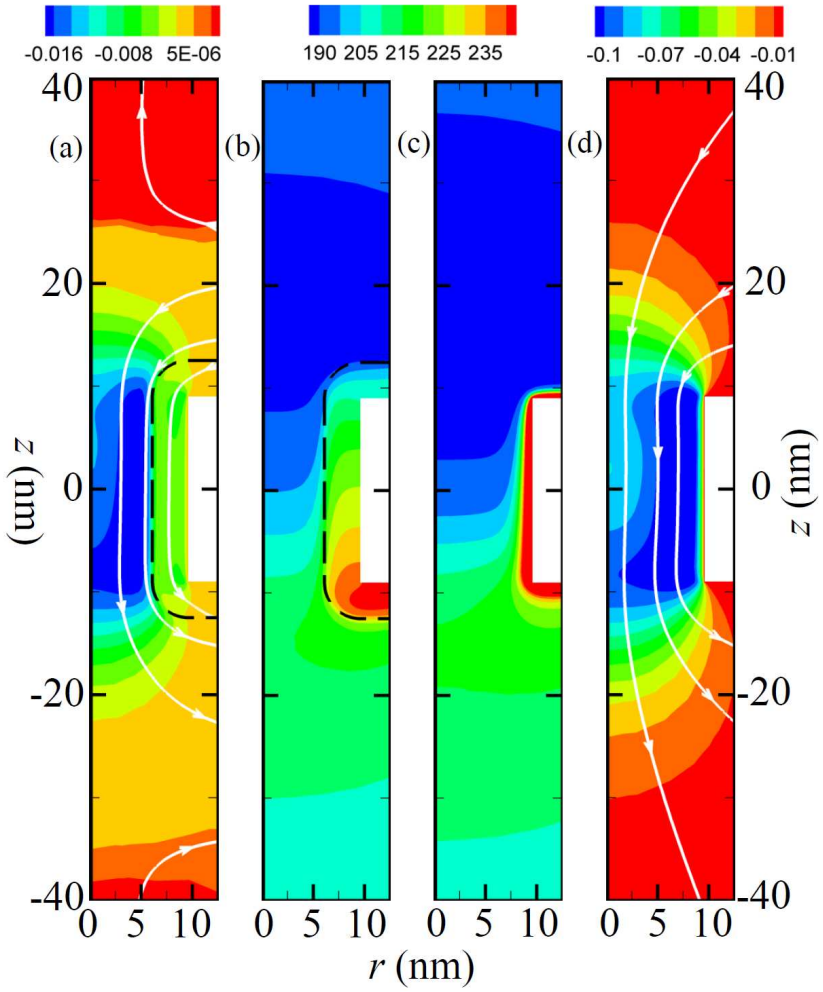

Figure S3. Flow field, (a), spatial distribution of the net cation concentration ($c_1 + c_2$), (b), for a PE-modified nanopore with the fixed charge density $\rho_{fix,w} = -4.57 \times 10^{-6}$ C/m^3 at $C_{\mathrm{KCl}} = 200$ mM. Other parameters are the same as those in Figure 4a of the text. Dashed curves: the outer boundary of the PE layer of the PE-modified nanopore. (c) and (d) denote the corresponding results of ($c_1 + c_2$) and the flow field, respectively, for a solid-state nanopore of surface charge density σ_w. The net amounts of charge carried in both cases are the same at $\rho_{fix,w} \times \Phi_{\mathrm{PE}} = \sigma_w \times \Delta_{\mathrm{solid}}$ with Φ_{PE} and Δ_{solid} being the volume of the PE layer in the PE-modified nanopore and the surface area of the solid membrane, respectively. Color

bars in (a) and (d): axial fluid velocity; streamlines with arrows: fluid velocity vector.

4. Influences of the Softness Degrees (λ_w and λ_p)

Figure S4 illustrates the influences of the softness degrees of the PE layer in the PE-modified nanopore λ_w, (a) and (c), and the soft layer in the soft NP λ_p, (b) and (d), on the translocation velocity of the soft NP, u_p, and the corresponding ionic current deviation χ. In general, a small softness degree implies that the molecular chain structure in an ion-penetrable soft layer is compact (or ordered). Similar to the results in Figure 4a and b in the text, Figure S4a and b reveals that the capture velocity of the soft NP can be enhanced before entering the PE-modified nanopore (arrows), that is, it becomes easier to thread the nanopore. As stated in the discussion of Figure 4a and b, this can be attributed to a significant cations-rich CP occurring at the PE-modified nanopore mouth. Figure S4a and b also indicates that if λ_w is sufficiently large and/or λ_p is sufficiently small, u_p is negative before the soft NP enters the PE-modified nanopore (blue region), implying that it is trapped there. The former is because the friction force stemming from the PE layer of the PE-modified nanopore increases with increasing λ_w, thereby strengthening the EOF and making it harder for the soft NP to pass through the nanopore. The latter can be explained by that the smaller the λ_p the greater the hydrodynamic drag coming from the EOF inside the soft layer of the NP and, therefore, a greater driving force is required to drive the soft NP into the nanopore. Figure S4c and d reveals that, regardless of the levels of λ_w and λ_p, a current

blockade is always present at $C_{\mathrm{KCl}} = 200\,\mathrm{mM}$, which is consistent with the result in Figure 4c of the text. Figure S4c and d also shows that although the influences of λ_w and λ_p on u_p are significant, the ionic current signature (current blockade) are almost independent of the hydrodynamic softness degrees of the ion-penetrable layers. This implies that the proposed PE-modified nanopore is capable of controlling the translational velocity of the soft NP, so that the sensing resolution and performance can be enhanced, without affecting its basic ionic current signature.

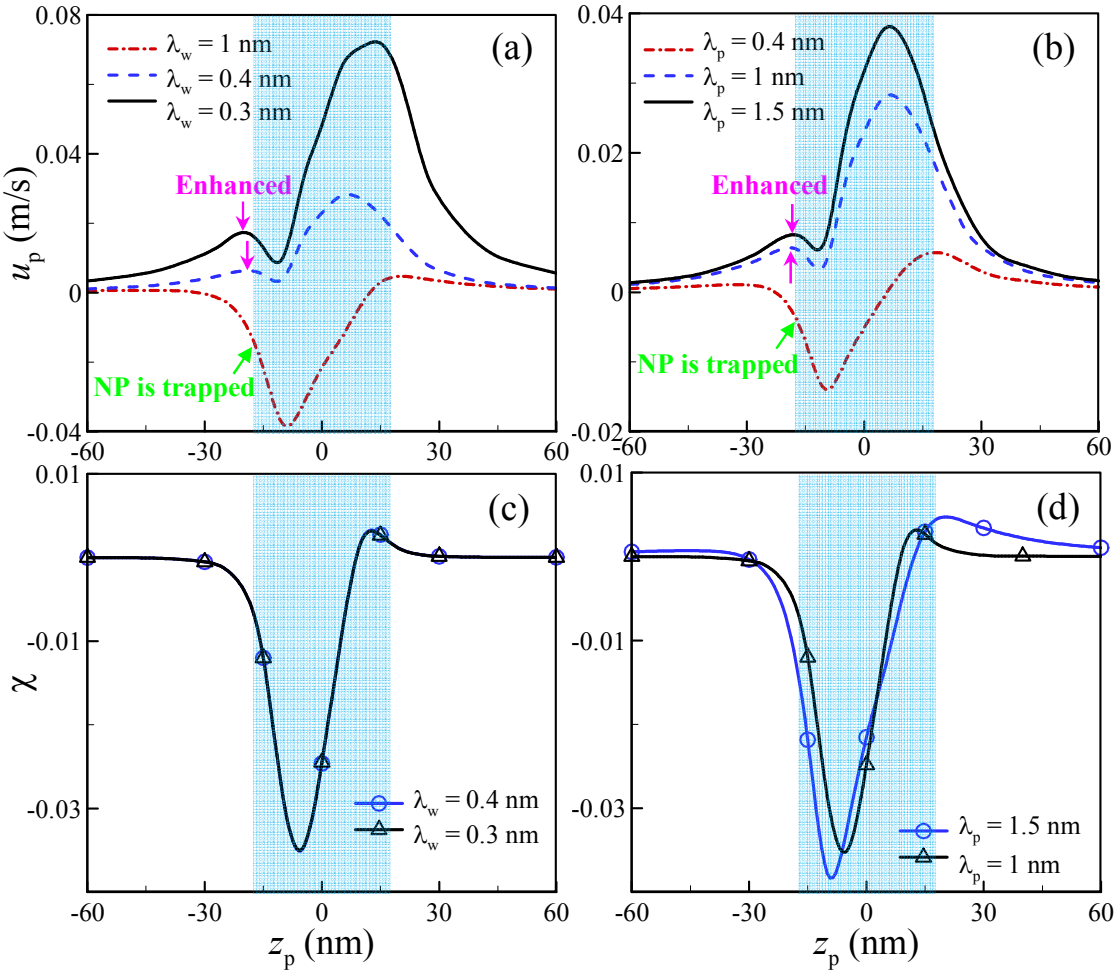

Figure S4. Particle translocation velocity, (a) and (b), and the corresponding ionic current

deviation, (c) and (d), as a function of the particle position z_p for various softness degrees of the soft layer in the PE-modified nanopore λ_w, (a) and (c), and those of the PE layer in the soft NP λ_p, (b) and (d), for the case where the background solution pH_0=7.5, the background salt concentration $C_{\mathrm{KCl}} = 200\,\mathrm{mM}$, and the nanopore length $L_N = 18\,\mathrm{nm}$. (a) and (c): $\lambda_p = 1\,\mathrm{nm}$; (b) and (d): $\lambda_w = 0.3\,\mathrm{nm}$. Blue regions ($-17.5\,\mathrm{nm} \le z_p \le 17.5\,\mathrm{nm}$) highlight the region where the soft NP locates in the PE-modified nanopore; curves in (c) and (d) show the results for the cases where the soft NP is able to pass through the nanopore.

5. Influence of Nanopore Length

The length of a nanopore plays an important role in its sensing applications. In Figure 4a and b of the text, we find that the smallest u_p inside the PE-modified nanopore (blue region) occurs when the NP's center of mass approaches the entrance of the nanopore (i.e., $z_p \cong -L_N/2$). If this smallest u_p, defined as $u_{p,c}$, is positive, the soft NP is capable of overcoming the access barrier and, therefore, enters the nanopore, implying that the sensing of a single molecule can be achieved. The influences of the background salt concentration C_{KCl} and pH_0 on $u_{p,c}$ for two values of nanopore length L_N are depicted in Figure S5. Similar to the results seen in Figure 4, if $u_{p,c}$ is positive, it increases with increasing C_{KCl} and/or pH_0. In addition, the turning point of $u_{p,c}$, the value of $u_{p,c}$ at which its sign changes from negative to positive, also increases with increasing C_{KCl} and pH_0. This implies that a higher C_{KCl} or pH_0 is required for a soft NP to overcome the access barrier so that it can enter the nanopore (see relevant discussion of Figure 4a and b of the text). In addition to

observing a current blockade signal, this also explains that nanopore-based single biomolecule sensing experiments often conducted at a high salt concentration to ensure that biomolecules are capable of entering the nanopore. It is interesting to note that if L_N is small, $u_{p,c}$ is less dependent on C_{KCl} or pH_0, and a lower pH_0 is required to overcome the access barrier. Since the imposed potential bias V_o is fixed and most of the potential drop occurs inside the nanopore, the enhanced electric field inside the nanopore increases with decreasing L_N, so is the electrophoretic driving force. On the other hand, because the net amount of charge in the PE layer of the PE-modified nanopore decreases with decreasing L_N, so is the strength of the associated EOF. The behavior of $u_{p,c}$ at small L_N results from these two competing effects.

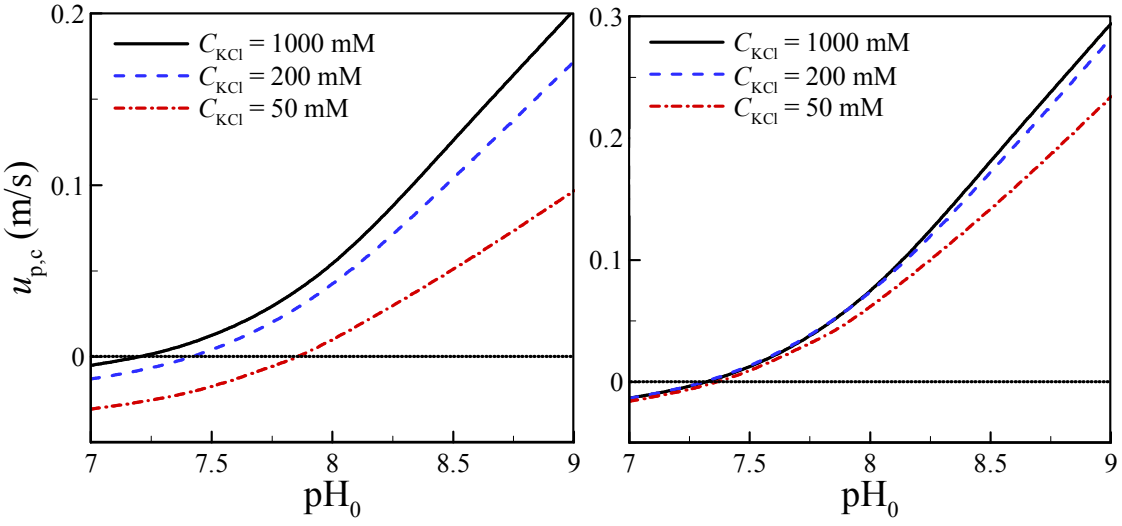

Figure S5. Critical particle translocation velocity $u_{p,c}$ as a function of the background solution pH_0 for various levels of background salt concentrations C_{KCl} at $z_p = -10$ nm and $L_N = 18$ nm, (a), and that at $z_p = -5$ nm and $L_N = 5$ nm (b).

REFERENCES

(1) Ai, Y.; Liu, J.; Zhang, B. K.; Qian, S. *Anal. Chem.* **2010**, *82*, 8217-8225.

(2) Ohshima, H. *Adv. Colloid Interface Sci.* **1995**, *62*, 189-235.

(3) Zhang, M. K.; Ai, Y.; Kim, D. S.; Jeong, J. H.; Joo, S. W.; Qian, S. Z. *Colloid Surf. B-Biointerfaces* **2011**, *88*, 165-174.

(4) Yeh, L. H.; Zhang, M. K.; Qian, S. Z.; Hsu, J. P. *Nanoscale* **2012**, *4*, 2685-2693.

(5) Ai, Y.; Zhang, M. K.; Joo, S. W.; Cheney, M. A.; Qian, S. Z. *J. Phys. Chem. C* **2010**, *114*, 3883-3890.

(6) Ohshima, H. *Electrophoresis* **2006**, *27*, 526-533.

(7) Yeh, L. H.; Hsu, J. P. *Soft Matter* **2011**, *7*, 396-411.

(8) Yeh, L. H.; Zhang, M.; Qian, S.; Hsu, J. P.; Tseng, S. *J. Phys. Chem. C* **2012**, *116*, 8672-8677.

(9) Yeh, L. H.; Liu, K. L.; Hsu, J. P. *J. Phys. Chem. C* **2012**, *116*, 367-373.